Faraday Discussions

Cite this: *Faraday Discuss.*, 2023, **247**, 216

PAPER

Core–shell nanostructured Cu-based bi-metallic electrocatalysts for co-production of ethylene and acetate

Jeannie Z. Y. Tan, * Ashween Kaur Virdee, John M. Andresen and M. Mercedes Maroto-Valer

Received 3rd March 2023, Accepted 19th June 2023
DOI: 10.1039/d3fd00058c

Direct electrocatalytic CCU routes to produce a myriad of valuable chemicals (*e.g.*, methanol, acetic acid, ethylene, propanol, among others) will allow the chemical industry to shift away from the conventional fossil-based production. Electrofuels need to go beyond the current electroreduction of CO_2 to CO, and we will here demonstrate the continuous flow electroreduction of syngas (*i.e.*, CO and H_2), which are the products from CO_2-to-CO, with enhanced product selectivity (~90% towards ethylene). To overcome current drawbacks, including bicarbonate formation that resulted in low CO_2 utilisation and low C_{2+} product selectivity, the development of nanostructured core–shell bi-metallic electrocatalysts for direct electrochemical reduction of syngas to C_{2+} is proposed. Electrosynthesis of ethylene is performed in a state-of-the-art continuous flow three-compartment cell to produce ethylene (cathodic gas phase product) and acetate (cathodic liquid phase product), simultaneously.

1. Introduction

Meeting the Paris Agreement[1] will require a wide range of mitigation and removal strategies, among which carbon capture and utilization (CCU) is particularly appealing as it can curb emissions while creating economic value. Notably, according to estimates, the large-scale deployment of CCU could help to decarbonise industrial activities by saving up to 3.5 $GtCO_{2eq}$ per year in 2030, that is, an 83% reduction compared with conventional fossil-based technologies.[2] Chemical industry is one of the top three emitting industries and is among the most difficult to decarbonise. The most effective way to decarbonise the chemical industry is to reduce the reliance on fossil fuels and gas demand as the feedstocks to the sector as the largest-volume chemicals to produce commodity chemicals to satisfy global markets. In addition, fossil fuels are also used to provide heat and pressure to drive those chemical reactions.

Research Centre for Carbon Solutions (RCCS), Heriot-Watt University, Edinburgh, EH14 4AS, UK. E-mail: j.tan@hw.ac.uk

Amongst the commodity chemicals, acetic acid, ethylene and ethylene glycol (6.5, 164 and 30.2 Mt per year, respectively) are the most important chemicals for the chemical and pharmaceutical sectors. Ethylene as the major platform chemical has a global production increased from 185 Mt in 2018 to 214 Mt in 2021 and the average price of ethylene worldwide has increased to 1235 USD per ton.[3] Unfortunately, it is produced *via* steam cracking of naphtha, currently the predominant production route followed by the thermal cracking of ethane,[4] that emits 1.51 $kgCO_{2eq}\ kg^{-1}$ of ethylene (cradle-to-gate),[5] resulting in 0.26 $GtCO_{2eq}$ (in order to satisfy the 2021 production volume) and accounting for 30% of the total energy needs of the chemical industry.[6]

CO_2 electrochemical reduction (CO2RR) into value added products using renewable energy offers a promising approach to reduce anthropogenic CO_2 emissions and development of sustainable energy systems. Coupling the intermittent electricity generated from solar and wind energy for CO2RR has been explored extensively for storing renewable electricity in chemicals, such as ethylene. CO2RR can produce carbon monoxide (CO), methane (CH_4), methanol (CH_3OH), formic acid (HCOOH), ethylene (C_2H_4) ethanol (CH_3CH_2OH) and chemicals with longer chain hydrocarbons. However, implementations of this technology for large-scale applications are challenging as the molecule is thermodynamically stable. Some other bottlenecks, including carbonate formation, poor product selectivity, low carbon utilisation rate, competition of H_2 evolution reaction at low potentials, and poor stability, need to be overcome to make low temperature CO2RR competitive with other CO_2 conversion technologies or chemical and energy production processes.[7]

Cu is the only electrocatalyst with acceptable activity and selectivity for C_{2+} products due to the unique property of binding *CO and *H.[8] However, CO2RR requires a high bias (approx. −1.0 V *vs.* reversible hydrogen electrode, RHE). Furthermore, under high biases (−0.9 to −1.1 V) up to 12 different C2 or C3 products can be identified at the Cu polycrystalline cathode.[9] To improve the efficiency and selectivity of C_{2+} products, the alkaline flow electrolyser has been proposed because it is one of the best electrolysers with high faradaic efficiency (90%) as well as superior single pass conversion efficiency (40%).[10] However, the electrolyser consumes a lot of the electrolyte due to reductive disproportionation into CO and CO_3^{2-}. As a result, the CO_2 utilisation rate is significantly limited, and large voltage is required.[7] To date, the best performing electrolyser for CO_2 to ethylene displayed a 15% energy efficiency, 2% carbon efficiency, 60 h of steady state operation at 3.5 V and 500 mA cm^{-2}.[11]

Addressing the carbonate formation is vital for this technology to make it a viable option for renewable chemical and fuel production. To date, the best reported CO production performance could be achieved at 3 V with approx. 4000 h at steady state operation under 200 mA cm^{-2} with 98% product selectivity.[12] The carbon efficiency reported is 43%. With this outstanding performance of CO production, the production of C_{2+} products in the sequential step needs to be developed to produce more valuable products, such as ethylene and acetic acid, which are ~$1200 and ~$800 per Mt in 2021. Furthermore, the electro-conversion of these C_{2+} products are among the potential commodity chemicals with high revenue.[10] Hence, the optimisation of the co-production of these commodity chemicals is the aim of the first part of this study.

The use of bimetallic electrocatalysts has been proposed previously to enhance the product selectivity with low overpotential required. For instant, Wang *et al.* reported that bimetallic Cu–Ag nanoflowers showed enhanced product selectivity towards acetaldehyde (~70%) from CO at −0.536 V *vs.* RHE.[13] Kuhn *et al.* also pointed out that a Cu–Ag bimetallic electrocatalyst had shown enhanced product selectivity towards ethylene (43% at −0.75 V *vs.* RHE) due to increased conductivity, stability and concentration of adsorbed CO when compared to Ag and Cu single metallic electrocatalysts.[14] Furthermore, Gao *et al.* demonstrated that the Cu–Co core–shell bimetallic electrocatalysts with Co-rich samples were more selective towards hydrocarbons, whereas Cu-rich samples were prone to produce oxygenated compounds from syngas.[15] Herein, three types of core–shell bimetallic electrocatalysts were synthesized. The syngas conversion performances of these electrocatalysts were analysed as the second part of this study.

2. Experimental

2.1 Chemicals

Oleylamine (OAm, R&D grade); copper nanoparticles ($Cu_{Ref.}$, 60–80 nm, ≥99.5%); copper(II) acetylacetonate ($Cu[acac]_2$, ≥99.9%); palladium(II) trifluoroacetate ($Pd[OCOCF_3]_2$, 97%); silver trifluoroacetate ($AgOCOCF_3$, 98%); tetrahydrofuran (THF, anhydrous ≥99.9%); isopropanol (IPA, ACS reagent ≥99.5%); Nafion™ (20 wt%) and dimethyl sulfoxide (DMSO, ≥99.9%) were purchased from Sigma-Aldrich. Potassium hydroxide (KOH, 85%) was purchased from Acros. Methanol (HPLC grade ≥99.8%); hexane (HPLC grade ≥95%) and deuterated water (D_2O) were purchased from Fisher Chemical. Diphenyl ether (DPE) and cobalt(II) acetylacetonate ($Co[acac]_2$, ≥99.0%) were purchased from Merck. All chemicals were used without further purification. Carbon gas diffusion layer (GDL) was Teflonated Toray TGP-60 from Alfa Aesar GmbH & Co; nickel foam (Nanoshel, 99.9%). Milli Q water (18 ΩM) was used throughout the study.

2.2 Methods

2.2.1 Synthesis of Cu nanoparticles (Cu_{core}). The synthesis of Cu_{core} followed a previous published report.[14] Briefly, the growth of the Cu_{core} nanoparticles was achieved in a single pot under a CO gas environment. 16 mg of $Cu(acac)_2$ was dissolved in OAm (9 mL) in a three-neck flask. Then, DPE (120 μM) was added into the resulting turquoise-blue solution, which was placed in an oil bath at 25 °C with continuous stirring throughout the following steps. A Schlenk line was connected with N_2, CO and a vacuum pump (KNF, Model: N86KT.18). Before switching to N_2, the line was held under vacuum for 5 min to remove the air from the system. This process was repeated for 4 times. CO was then introduced into the system at a flow rate of 5 mL min^{-1} throughout the following steps. Caution: CO is toxic and should be handled with extra care in a well-vented chemical hood equipped with a CO detector. The temperature was maintained at 30 °C for 30 min, followed by heating to 220 °C with a ramp rate of 1.6 °C min^{-1} using the oil bath. The colour of the solution changed from transparent blue green to yellow to reddish-brown during heating. The temperature of the solution was kept at 220 °C for 2 h before letting it cool down to 25 °C naturally.

2.2.2 Synthesis of core–shell bi-metallic nanoparticles. The synthesis of bi-metallic core–shell nanoparticles followed a previous published report.[14] Briefly, an $AgOCOCF_3$, $Co[acac]_2$ or $Pd[OCOCF_3]_2$ solution was prepared by adding pre-determined amount of OAm (2 mg mL^{-1}) in a 10 mL vial. The vial was sonicated for 30 min to ensure the salt was completely dissolved. A syringe pump (Kent Scientific, Model: Genie Touch) was used to inject 5 mL of the resulted salt solution into the three-neck flask that contained the suspension of Cu_{core} at 30 °C while CO was flowing. The infusion rate of the metal (*i.e.*, Ag, Co or Pd) precursor was set at 0.5 mL h^{-1} to ensure uniform growth of the shell layer. After 5 mL of the metal precursor solution was added, the mixture was kept under stirring for another 12 h while maintaining the temperature at 30 °C and a flowrate of CO gas at 5 mL min^{-1}. The formed NPs were collected by centrifuge (Eppendorf 5810) at 11 000 rpm for 3 min, followed by washing with hexane as the dispersing agent (3 mL) and methanol as the antisolvent (17 mL). The samples, labelled as Cu@Ag, Cu@Co or Cu@Pd, were dispersed in hexane for further use.

2.2.3 Preparation of electrodes. The cathode catalysts were deposited *via* hand-painting onto a carbon GDL. 2 mg of $Cu_{Ref.}$ sample was mixed with THF (200 μL), IPA (200 μL), and Nafion (5.2 μL). The solutions were sonicated for 1 h to obtain a homogeneous ink. The ink was then hand-painted using an airbrush on the GDL at a loading of 1.0 mg cm^{-2}. This procedure was repeated for the Cu_{core}, Cu@Ag, Cu@Co and Cu@Pd electrocatalysts.

2.3 Electrocatalytic testing

The electroreduction of syngas (CO/H_2) was tested using an alkaline flow cell setup (Fig. 1). Gaseous CO/H_2 (varied with different ratio) was continuously supplied to the back of the cathode at various rates controlled by a mass flow control (Bronkhorst EL-Flow Select). A syringe pump continuously fed KOH (refer to Table 1) as the catholyte and anolyte through two silicone rubber (SiloCell White from Polymax, 9 mm thickness) electrolyte chambers separated by an anion exchange membrane (AEM, AHA Membrane from Eurodia Ltd). The cell

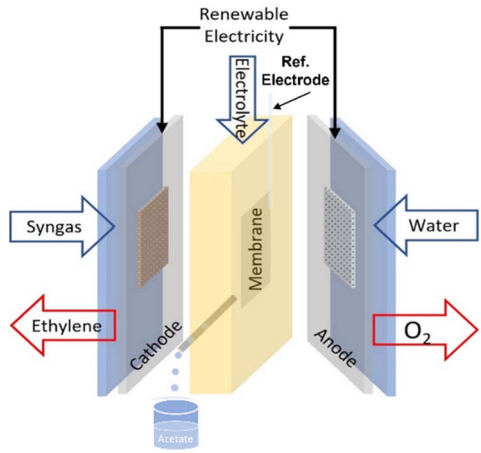

Fig. 1 Schematic diagram of the alkaline flow cell setup.

Table 1 Parameters manipulated in DOE using commercially manufactured Cu nanoparticles

Run no.	$CO:H_2$	Concentration KOH (M)	Flowrate (mL min^{-1})
1	1 : 0	0.1	0.54
2	1 : 1	0.1	0.41
3	1 : 0	0.1	1.07
4	1 : 1	0.1	1.07
5	1 : 0	2.0	0.54
6	1 : 1	2.0	0.41
7	1 : 0	2.0	1.07
8	1 : 1	2.0	1.07
9	1 : 1	1.0	0.78

potential was varied *via* a potentiostat (Autolab PGSTAT302N) and the corresponding current density was continuously measured. Multimeters hooked up to the flow cell were used to measure cathode and anode potentials against an Ag/AgCl reference electrode (Ossila, C2015B1). For a typical procedure, the cell was first hooked up to the CO and/or H_2 feed, electrolyte pump, potentiostat, multimeters, and gas chromatograph (GC, Agilent Technologies 7890B equipped with TCD-FID detectors). Each experiment was begun with two successive linear sweeps between −1.0 and −1.8 V *versus* Ag/AgCl to ensure proper functioning of the cell. The linear sweeps were followed by a potentiostatic preconditioning step at −1.0 V *versus* Ag/AgCl for 60 s. The cell was then stepped galvanostatically with one potentiostat and the cathode potentials were measured *versus* the Ag/AgCl reference electrode. Each galvanostatic step was 9 min in duration. Electrochemical impedance spectroscopy (EIS) measurements were conducted with the frequency range from 100 kHz to 0.1 Hz with an amplitude of 0.1 mA. Ten points were recorded per frequency decade.

2.4 Characterisation

The morphology of the synthesized products was examined using a field emission scanning electron microscope (FE-SEM, Quanta 200 F FEI), a high-resolution transmission electron microscope (HRTEM, FEI Titan Themis 200) equipped with an energy-dispersive X-ray spectroscopy (EDX) detector operated at 200 kV. To investigate the interior structures of the nanospheres, samples were embedded in TAAB 812 resin and sliced into ~90 nm thick sections. The sliced sections were mounted on the TEM Ni grid. Crystallinity and phase identification of the synthesized products were conducted using powder X-ray diffraction XRD (Malvern Panalytical Empyrean Diffractometer) equipped with Cu Kα radiation (λ = 1.5418 Å) and compared with the ICDD-JCPDS powder diffraction file database. Nuclear magnetic resonance spectroscopy (NMR, Bruker AVIII-400) was used to analyse the liquid products. Typically, 100 μL of the catholyte sample was mixed with 100 μL of DMSO standard solution and 400 μL of D_2O in an NMR tube. The DMSO standard solution was made by diluting the DMSO with D_2O to obtain the final concentration (1.262 mM). The samples were analyzed using ^1H NMR equipped with solvent suppression. The spectra were integrated and compared against a DMSO standard to quantify the concentrations of the liquid products.

3. Results and discussion

The electroreduction of syngas parameters were optimised through a series of experiments using design of experiment (DOE). A blank GDL was loaded onto the Cu flow plate and the experiment was run following the procedure above. No observable product was detected based on the GC and NMR results.

The parameters, including the concentration of electrolyte (*i.e.*, 0.1, 1 and 2 M), ratio of CO : H_2 and flow rate of syngas (Table 1), were manipulated to optimise the parameters for the electrocatalytic process. Using the stepped galvanostatic reduction method, the current applied was manipulated ranging from 1.0 to 4.5 mA. Each step (0.5 mA) was held for 9 min to allow sufficient time for sampling into GC. The optimised current applied was determined with the highest ethylene yielded from syngas. The experimental results were tabulated, and a Pareto chart was used to visualise the most significant factor in the DOE (Fig. 2). The Pareto chart revealed that the concentration of the electrolyte was the most significant factor affecting ethylene production efficiency. Meanwhile, −2.5 mA was the optimised applied current that resulted in the highest single pass production of ethylene, which was ~2.5 mM cm^{-2}.

Electronic impedance analysis was performed to justify the role of H_2 in the electroreduction of CO to ethylene (Fig. 3a). The Nyquist plot was obtained for commercial Cu being exposed to different gases, namely N_2, CO–N_2, CO–H_2 and CO. In particular, the high frequency process was found to be not dependent on electrode material and applied current; on the contrary the low frequency one was different for the measurements under different gases and highly dependent on the current applied. The former was attributed to the ionic migration toward the reaction site, whereas the latter reflected the charge transfer due to the reduction reaction.[16] The charge transfer resistance (R_{ct}) was found to be decreasing in the order of N_2 > CO > CO–N_2 > CO–H_2. When CO and CO–N_2 were introduced into the electrolyser, the reduction of R_{ct} was not significant. However, the exposure under CO–H_2 largely decreased R_{ct}. This result was attributed to the strong reducing

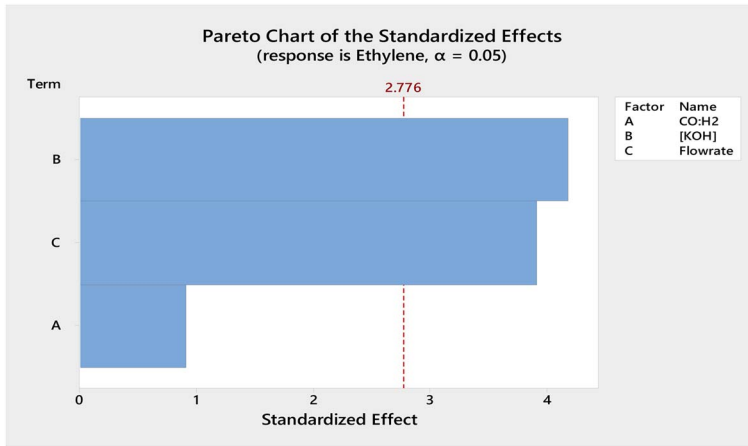

Fig. 2 Pareto chart of the standardized effects obtained for the factorial design optimization of the variables (A) CO : H_2, (B) concentration of KOH, and (C) flowrate of syngas.

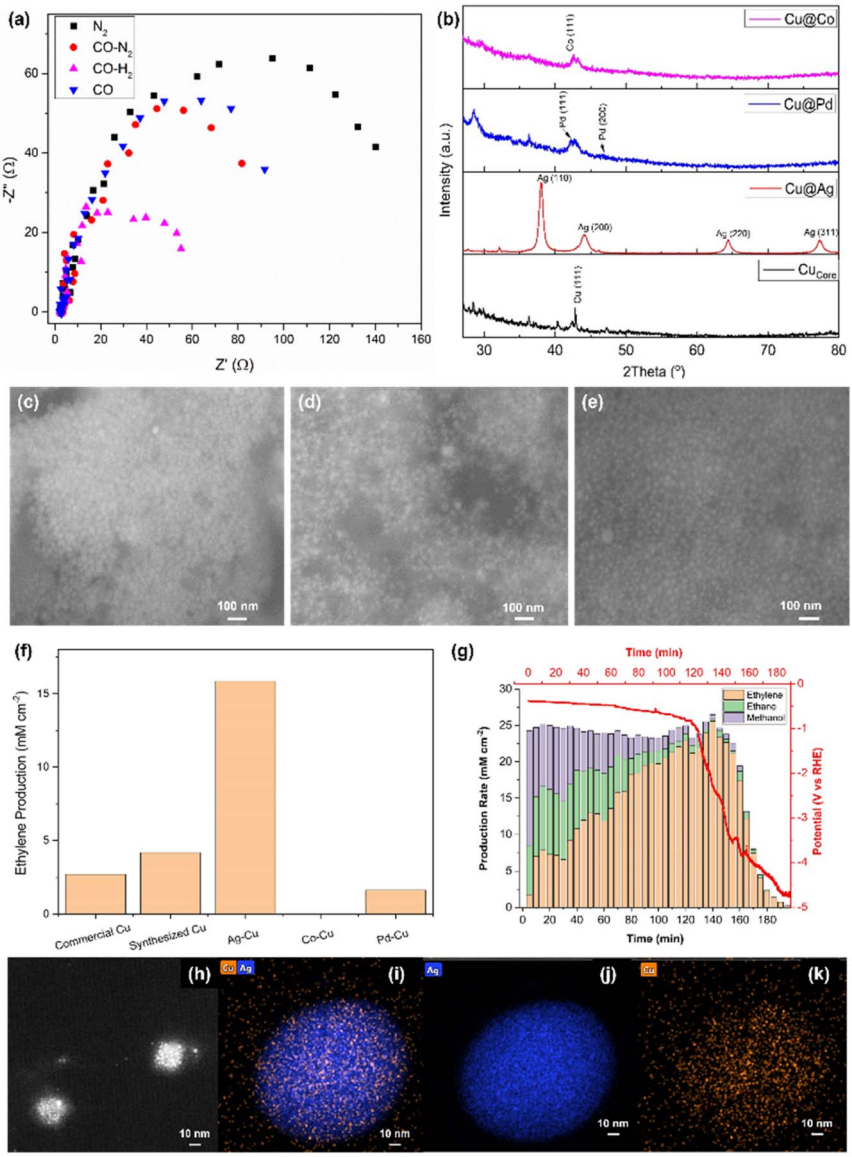

Fig. 3 (a) Impedance (Nyquist plot) of the commercial Cu measured in the presence of N_2 (black ■), $CO : N_2 = 1 : 1$ (red ●), $CO : H_2 = 1 : 1$ (magenta ▲), and CO only (blue ▼) under −2.5 mA of applied current and a total flow rate of 0.78 mL min^{-1}. (b) XRD pattern of synthesized Cu_{core} (black), Cu@Ag (red), Cu@Pd (blue) and Cu@Co (magenta). SEM images of (c) Ag@Cu, (d) Pd@Cu and (e) Co@Cu. HRTEM of (h) synthesized Cu_{core} and (i) Ag@Cu with elemental mapping of (j) Ag and (k) Cu. (f) Single pass ethylene production rate using commercial Cu, synthesized Cu_{core}, Ag@Cu, Co@Cu and Pd@Cu. (g) Stability test of Ag@Cu under 2.5 mA for 200 min.

power of CO and H_2. When CO and/or H_2 were introduced into the electrolyser, the oxidised Cu electrocatalyst was reduced to Cu. Being a stronger reducing agent, H_2 tended to reduce more O_2 that adsorbed on the electrocatalyst

compared to CO, providing more electrochemically active area, thus, enhancing the conductance.[17] Furthermore, a recent study concluded that the adsorption of H_2 would reconstruct the surface Cu atoms in the electroreduction conditions based on the simulation, thus, reducing the potential barrier.[18]

The optimised experimental conditions, which were 1 : 1 CO : H_2, 1.0 M of KOH and 0.78 mL min^{-1} of syngas, were applied for the following experiments using different bi-metallic electrocatalysts. The flow of electrolyte was maintained at 0.15 mL min^{-1}.

Three different types of bi-metallic electrocatalysts were synthesized using the sol–gel method as detailed in the experimental procedure section 2.2.2. The crystallinity of the synthesized electrocatalysts was evaluated using XRD (Fig. 3b). The synthesized Cu_{core} with metallic dark brownish colour showed a very weak XRD signal probably due to the small nano-crystallite size. When Ag was loaded as the shell layer, Ag metal produced a strong XRD pattern at 38.1, 44.2, 64.4 and 77.4°, which corresponded to (110), (200), (220) and (311) phases, respectively. Pd and Co were also synthesized as the shell materials of Cu_{core} using the same experimental conditions. Unfortunately, the XRD patterns of these metals were very broad and poor compared to Ag although the Pd (111), Pd (200) and Co (111), which were located at 42.3, 47.0 and 42.6°, respectively, were identified. This was due to very small nanocrystallite size deposited on Cu_{core}.

The morphology of the nanoparticles was characterised using SEM. The synthesized samples appeared as very small nanoparticles. The synthesized Cu_{core} was hardly seen under SEM, thus, the TEM image of Cu_{core} was provided (Fig. 3h). The highly crystallized Ag@Cu revealed the largest particle size (~25 nm, Fig. 3c) among the bi-metallic electrocatalysts (*i.e.*, ~15 and ~12 nm for Pd@Cu and Co@Cu (Fig. 3d and e), respectively).

The synthesized electrocatalysts were used as the cathodic material in the tailor-made alkaline flow cell using the optimised conditions. Each sample was tested using the galvanostatic method as detailed in DOE experiments. The single conversion efficiency of Ag@Cu was the highest among the samples, which was ~15.0 mM cm^{-2}, when 2.5 mA was applied. Meanwhile, Cu_{core} produced ~4.9 mM cm^{-2}, followed by commercial Cu (~2.5 mM cm^{-2}) and Pd@Cu (~2 mM cm^{-2}, Fig. 3f). Unfortunately, Co@Cu showed trace amount of ethylene production. The underperforming of Co@Cu and Pd@Cu was due to the strong electronegativity of Ag compared to Co and Pd. In addition, the low crystallinity and coverage of the Co and Pd compared to Ag@Cu led to unsatisfactory performance.

To further understand the morphology of the synthesized Cu_{core} and Ag@Cu, HRTEM was utilised to examine these electrocatalysts. The synthesized Cu_{core} exhibited a self-assembled nanosphere with diameter ~10 nm that was formed from a group of nanoparticles (Fig. 3h). The elemental analysis on the electrocatalysts was conducted using EDX-HRTEM. The shell layer of Ag (Fig. 3i and j) exhibited a much stronger signal than Cu as the core material (Fig. 3k). This suggested that Ag had formed a thick, solid layer over the Cu.

The best performing sample Ag@Cu was used to perform a stability test. The current of −2.5 mA was supplied continuously to the cell, while the potential was measured simultaneously with the gas sampling through the connected GC. The production rate of ethylene was analysed and plotted (Fig. 3g, yellow bars). The production rate increased immediately after the first 5 min from 1 to ~7.5 mM cm^{-2} (10–30 min). The production rate was doubled after 40 min and stabilised at

$\sim$22 mM cm^{-2}. The maximum production rate achieved was 25 mM cm^{-2} at the 140th min before the measured potential started to descend. The potential dropped quickly and approached $-$4.8 V *vs.* RHE after 140 min. This had also resulted in the decrease of ethylene production concurrently and eventually approached 0. The overall ethylene selectivity was 75% with $\sim$15% of ethane (Fig. 3g, green bars) and 10% of methanol (Fig. 3g, purple bars) based on the gaseous product analysis using GC. The total production of ethylene in the single pass conversion was calculated to be 0.5 M after 180 min, which was $\sim$40% efficiency.

To elucidate the liquid products from the cathode compartment, the catholyte, which was flowing through the middle compartment throughout the experiment, was analysed using NMR (Fig. 4). The catholyte obtained was analysed without purification. The NMR spectrum revealed that acetate was the only product in the catholyte. No other by-product was detected. The concentration of acetate was estimated to be 2.65 g L^{-1}.

The impedance of Ag@Cu before and after the stability test was recorded as shown in the Nyquist plots (Fig. 5). The R_{ct} of the post-run sample increased 5–6 times when compared to the fresh sample. In addition, the post-run electrocatalyst revealed some white deposition on the GDE (inset of Fig. 5), which was due to the accumulation of acetate. Hence, the increase in R_{ct} was postulated to be due to the accumulation of acetate that increased the potential barrier and hindered the electrocatalytic sites. This explained the phenomenon of rapid reduction in products obtained from the electroreduction process after 140 min. The accumulation of acetate on the GDE over the time had also reduced and constrained the adsorption of CO on the GDE that probably shifted the product selectivity from methanol to ethylene as suggested by a recent study.[19]

The co-production of high selective ethylene from syngas in the gas compartment and potassium acetate in the middle compartment exhibited the advantage of the three-compartment electrolyser, in which the products in gas and liquid phases were prohibited to cross-over, which prevented the oxidation of reduced products. As a result, the product selectivity was promoted. Further enhancement of the single pass conversion efficiency with high product selectivity (*i.e.*, avoid product purification/separation processes) would significantly enhance the economic feasibility of the electrolyser for CCU applications.

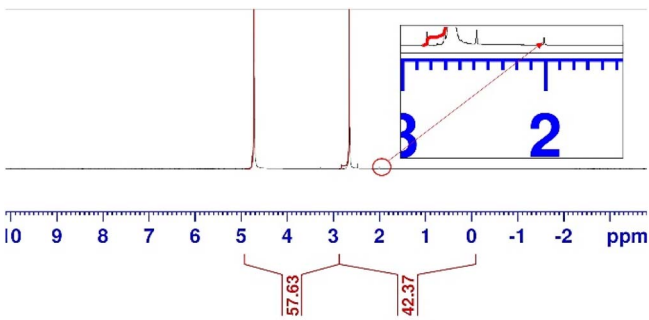

Fig. 4 NMR spectrum of the solution obtained after a single pass conversion from the middle compartment of the electrolyser.

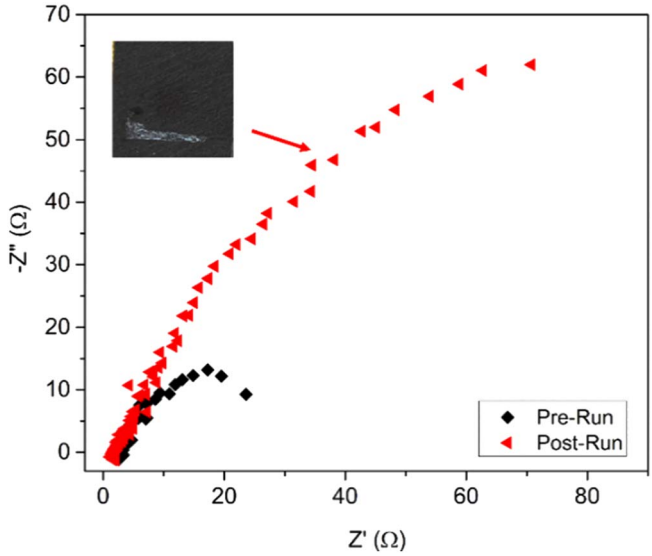

Fig. 5 Impedance (Nyquist plot) of Ag@Cu measured before (◆) and after (◀) the stability test.

4. Conclusions

A three-compartment alkaline flow-through electrolyser was successfully developed and the single pass conversion of syngas to ethylene achieved was 2.5 mM cm^{-2} in the optimised conditions (*i.e.*, 1 : 1 of $CO : H_2$; 1.0 M of KOH and 0.78 mL min^{-1} of total gas flow under −2.5 mA cm^{-2}). The single pass conversion of syngas to ethylene was dramatically enhanced when the fabricated core–shell Cu@Ag sample (15 mM cm^{-2}) was employed as the electrocatalyst, the co-production of ethylene (∼40%) and potassium acetate (2.65 g L^{-1}) was obtained as the gas and liquid products, respectively, with high purity (>70%). The impedance measurements suggested that the shifting of product selectivity from methanol to ethylene over the time and deterioration of ethylene production after 2 h were due to the accumulated acetate that hindered the electrocatalytic sites. Further mechanistic study and optimisation are required to fully understand the reaction pathways. Although the core–shell Cu–Ag bimetallic electrocatalyst showed promising conversion efficiency, the stability of ethylene production would need to be explored further.

Conflicts of interest

There are no conflicts to declare.

Acknowledgements

The authors/we would like to acknowledge that this work was supported by the UKRI ISCF Industrial Challenge within the UK Industrial Decarbonisation Research and Innovation Centre (IDRIC) award number: EP/V027050/1.

References

1 United Nations Framework Convention on Climate Change (UNFCCC), *Adoption of the Paris Agreement*, 2015.
2 A. Kätelhön, R. Meys, S. Deutz, S. Suh and A. Bardow, *Proc. Natl. Acad. Sci. U. S. A.*, 2019, **116**, 11187–11194.
3 **https://www.statista.com/statistics/1170573/price-ethylene-forecast-globally/**.
4 M. Ghanta, D. Fahey and B. Subramaniam, *Appl. Petrochem. Res.*, 2014, **4**, 167–179.
5 G. Wernet, C. Bauer, B. Steubing, J. Reinhard, E. Moreno-Ruiz and B. Weidema, *Int. J. Life Cycle Assess.*, 2016, **21**, 1218–1230.
6 E. Worrell, D. Phylipsen, D. Einstein and N. Martin, *Energy Use and Energy Intensity of the U.S. Chemical Industry*, 2000.
7 J. A. Rabinowitz and M. W. Kanan, *Nat. Commun.*, 2020, **11**, 5231.
8 A. Bagger, W. Ju, A. S. Varela, P. Strasser and J. Rossmeisl, *ACS Catal.*, 2019, **9**, 7894–7899.
9 A. R. Woldu, A. H. Shah, H. Hu, D. Cahen, X. Zhang and T. He, *Int. J. Energy Res.*, 2020, **44**, 548–559.
10 J. Sisler, S. Khan, A. H. Ip, M. W. Schreiber, S. A. Jaffer, E. R. Bobicki, C.-T. Dinh and E. H. Sargent, *ACS Energy Lett.*, 2021, **6**, 997–1002.
11 F. P. García de Arquer, C.-T. Dinh, A. Ozden, J. Wicks, C. McCallum, A. R. Kirmani, D.-H. Nam, C. Gabardo, A. Seifitokaldani, X. Wang, Y. C. Li, F. Li, J. Edwards, L. J. Richter, S. J. Thorpe, D. Sinton and E. H. Sargent, *Science*, 2020, **367**, 661–666.
12 Z. Liu, H. Yang, R. Kutz and R. I. Masel, *J. Electrochem. Soc.*, 2018, **165**, J3371.
13 L. Wang, D. C. Higgins, Y. Ji, C. G. Morales-Guio, K. Chan, C. Hahn and T. F. Jaramillo, *Proc. Natl. Acad. Sci. U. S. A.*, 2020, **117**, 12572–12575.
14 A. N. Kuhn, H. Zhao, U. O. Nwabara, X. Lu, M. Liu, Y.-T. Pan, W. Zhu, P. J. A. Kenis and H. Yang, *Adv. Funct. Mater.*, 2021, **31**, 2101668.
15 W. Gao, Y. Zhao, H. Chen, H. Chen, Y. Li, S. He, Y. Zhang, M. Wei, D. G. Evans and X. Duan, *Green Chem.*, 2015, **17**, 1525–1534.
16 A. Sacco, *J. CO2 Util.*, 2018, **27**, 22–31.
17 D. P. Nagmani, A. Tyagi, T. C. Jagadale, W. Prellier and D. K. Aswal, *Appl. Surf. Sci.*, 2021, **549**, 149281.
18 Z. Zhang, Z. Wei, P. Sautet and A. N. Alexandrova, *J. Am. Chem. Soc.*, 2022, **144**, 19284–19293.
19 J. Li, Z. Wang, C. McCallum, Y. Xu, F. Li, Y. Wang, C. M. Gabardo, C.-T. Dinh, T.-T. Zhuang, L. Wang, J. Y. Howe, Y. Ren, E. H. Sargent and D. Sinton, *Nat. Catal.*, 2019, **2**, 1124–1131.

